Exploratory transcriptomics and *in vivo* analyses of suramin in tongue squamous cell carcinoma

WATARU KAKUGUCHI[1], MASAHIRO MORIMOTO[2], KENTA TAKAHASHI[1], NAKO MAISHI[3], KYOKO HIDA[3], TAKAO NOMURA[4], SATOKO OTSUGURO[4], KATSUMI MAENAKA[4] and YOICHI OHIRO[1]

[1]Department of Oral and Maxillofacial Surgery, Division of Oral Pathobiological Science, Faculty of Dental Medicine and Graduate School of Dental Medicine, Hokkaido University, Sapporo, Hokkaido 060-8586, Japan; [2]Division of Head and Neck, Cancer Institute Hospital, Japanese Foundation for Cancer Research, Tokyo 135-8550, Japan; [3]Department of Vascular Biology and Molecular Pathology, Division of Oral Pathobiological Science, Faculty of Dental Medicine and Graduate School of Dental Medicine, Hokkaido University, Sapporo, Hokkaido 060-8586, Japan; [4]Center for Research and Education on Drug Discovery, Faculty of Pharmaceutical Sciences, Hokkaido University, Sapporo, Hokkaido 060-0812, Japan

Received November 1, 2025; Accepted January 2, 2026

DOI: 10.3892/br.2026.2112

Abstract. Suramin, an anti-trypanosomal agent, has gained attention for its potential anticancer activity, partly through the modulation of RNA-binding proteins such as HuR. However, its genome-wide transcriptomic effects in oral squamous cell carcinoma remain unclear. In the present study, RNA-sequencing was performed on suramin-treated HSC-3 cells, followed by enrichment, network and transcription factor analyses. *In vivo* validation was conducted in an orthotopic xenograft model using luciferase-labeled HSC-3 cells. Suramin was administered intraperitoneally at a dose of 20 mg/kg, twice weekly. Transcriptomic profiling revealed broad downregulation of genes governing cell cycle progression, chromatin organization and DNA damage response, including mitotic regulators such as G_2/M regulators *CCNB1*, *CDC20* and *AURKA*, and their upstream transcription factors *FOXM1* and *MYBL2*. By contrast, genes associated with extracellular matrix remodeling (the MMP family and *TIMP3*) and stress or immune responses (*TXNIP* and *TNFSF10*) were upregulated. Functional enrichment confirmed the suppression of proliferative programs with the concurrent activation of tumor-suppressive microenvironmental responses. *In vivo*, suramin-treated mice exhibited lower tumor growth compared with that in the control group, although the difference was not statistically significant (P=0.18). Effect size estimates were relatively large for both the group effect (partial η^2=0.20) and the time x group interaction (partial η^2=0.24), suggesting that the study may have been underpowered to detect this difference statistically. In conclusion, the present exploratory study suggests that suramin exerts a dual antitumor effect on tongue squamous cell carcinoma by suppressing proliferative transcriptional programs, and modulating extracellular and stress response pathways, providing a basis for future studies to further elucidate its therapeutic relevance.

Correspondence to: Dr Wataru Kakuguchi, Department of Oral and Maxillofacial Surgery, Division of Oral Pathobiological Science, Faculty of Dental Medicine and Graduate School of Dental Medicine, Hokkaido University, Kita 13 Nishi 7, Kita, Sapporo, Hokkaido 060-8586, Japan
E-mail: wkakugu@den.hokudai.ac.jp

Key words: suramin, tongue squamous cell carcinoma, transcriptomics, orthotopic mouse model, cell cycle

Introduction

Tongue squamous cell carcinoma (TSCC), the most common oral cancer, demonstrates a strong tendency for cervical lymph node metastasis, even in the early stages (1). According to current National Comprehensive Cancer Network guidelines (Version 1.2026), standard treatment for head and neck squamous cell carcinoma, including TSCC, primarily involves surgical resection, with adjuvant radiotherapy or chemoradiotherapy for high-risk pathological features (2). In recent years, immune checkpoint inhibitors have been incorporated into the management of very advanced disease (unresectable, recurrent, or metastatic). Although therapeutic advances have been made, outcomes remain poor, particularly in patients with advanced or recurrent disease.

Suramin, a polysulfonated naphthylurea first developed in 1916 for African trypanosomiasis (3,4), has been repurposed for oncology due to its ability to block diverse signaling pathways (TGF-β, bFGF, PDGF, EGF, and VEGF) and cell cycle regulators (cyclins A2, B1, D1, and E). In addition, it interferes with the RNA-binding protein HuR, which stabilizes oncogenic transcripts (5-7).

These pleiotropic actions have renewed the interest in suramin and its use in hormone-refractory prostate cancer (HRPC) (8). At low doses, suramin can function as a chemosensitizer (4), and nanoparticle formulations combining suramin with doxorubicin have demonstrated strong efficacy without systemic toxicity in breast cancer models (9).

In TSCC, suramin suppresses tumor proliferation, migration, and invasion (7). However, clinical evidence remains limited, and the mechanisms underlying TSCC remain unclear. We investigated the effects of suramin on global gene expression in HSC-3 cells using next-generation sequencing (NGS) and evaluated its *in vivo* activity in a luciferase-labeled orthotopic mouse model to elucidate its therapeutic potential.

Materials and methods

Cell lines, cell culture, suramin treatment. The human tongue squamous cell carcinoma cell line HSC-3 (RIKEN, Tsukuba, Japan) and luciferase-expressing HSC-3 cells (HSC-3-Luc; JCRB Cell Bank, Osaka, Japan) were used. The cells were maintained in Dulbecco's Modified Eagle's medium (DMEM) supplemented with fetal bovine serum (FBS). Cells were incubated for 24 h in serum-free DMEM containing 100 μM suramin (FUJIFILM Wako Pure Chemical Corporation, Osaka, Japan). Control cells received an equivalent volume of UltraPure™ distilled water (Invitrogen; NY, USA), the solvent for suramin. The use of 100 μM suramin for 24 h was based on our previous report (7), in which this concentration effectively suppressed HuR-regulated genes, including *CCNB1* and *CCNA2*, at both the mRNA and protein levels while remaining non-cytotoxic in HSC-3 cells (IC_{50}=732 μM).

RNA extraction and sequencing. Total RNA was extracted using the RNeasy Mini Kit (Qiagen; Hilden, Germany), and 1 μg of total RNA was used for downstream processing. The mRNA was enriched with oligo (dT) beads, fragmented, and reverse-transcribed to generate cDNA. Library construction and sequencing were performed by Novogene (Beijing, China) using an Illumina platform.

Bioinformatics analysis. Raw reads were qualitatively checked and aligned to the human reference genome. Gene expression was quantified using HTSeq (v0.6.1, union mode) and normalized to fragments per kilobase of transcript per million mapped reads to enable comparisons between samples.

Differentially expressed genes (DEGs) were identified using DEGseq (10) with TMM normalization under a Poisson distribution model, and defined as those with $|\log_2$(fold change)$|$ >1 and q<0.005 (Benjamini-Hochberg false discovery rate). Gene Ontology (GO) and Kyoto Encyclopedia of Genes and Genomes (KEGG) enrichment analyses were performed using g:Profiler (version e113_eg59_p19_f6a03c19; database updated May 23, 2025). In GO analysis, terms with a size >1,500 were excluded, and categories with an intersection size ≥3 were retained; for KEGG, terms with a size <300 and an intersection size ≥3 were applied. Protein-protein interaction (PPI) networks were generated using STRING (version 12.0) with a high-confidence interaction threshold (combined score >0.700), and hub genes were identified by degree centrality. The DEGs were annotated using AnimalTFDB v4.0, and only sequence-specific transcription factors (TFs) were retained, excluding chromatin regulators and cofactors. Candidate transcription factors were further validated by confirming the binding motifs in JASPAR 2024 and by cross-referencing the binding activity with the ENCODE ChIP-seq datasets.

Biological replicates were not included, and this single-sample design limited statistical robustness; therefore, conservative DEG thresholds were applied to reduce false-positive findings.

Orthotopic tongue cancer mouse model and treatments. HSC-3-Luc cells ($1x10^5$) suspended in 30 μl of sterile HBSS (without calcium, magnesium, and phenol red; Gibco, Thermo Fisher Scientific, Waltham, MA, USA) were orthotopically injected into the left lateral tongue of 8-week-old male BALB/cAJcl-nu/nu mice using a 27-gauge needle. Day 0 was defined as the day of tumor implantation. Mice were anesthetized by intraperitoneal injection with a combination of medetomidine (Orion Pharma, Espoo, Finland), midazolam (Astellas Pharma, Tokyo, Japan), and butorphanol (Meiji Seika Pharma, Tokyo, Japan) (MMB) at doses of 0.6, 3.2, and 4.0 mg/kg, respectively. Because a previously reported intraperitoneal regimen of 0.75/4/5 mg/kg (11) resulted in deep anesthesia in preliminary experiments, an 80% reduced dose was employed in the present study. Because the procedure involved only intralingual injection, surgical-level deep anesthesia was not required, and adequate anesthesia was confirmed by the absence of body movement or facial response to gentle pinching with forceps or needle puncture of the tongue. The mice were randomized into three groups: vehicle (n=4), suramin 20 mg/kg (n=5), and suramin 60 mg/kg (n=4), which were administered intraperitoneally twice weekly. Tumor growth was monitored by bioluminescence imaging (BLI) using an IVIS Spectrum (PerkinElmer) on days 1, 8, 15, 22, 25, and 29 after intraperitoneal injection of VivoGlo™ Luciferin (150 mg/kg, 200 μl; Promega, Madison, WI, USA). Tumor growth was assessed on predefined imaging days (days 1, 8, 15, 22, and 29). An additional imaging session on day 25 was performed to assess tumor status because euthanasia was required at that time point. In this orthotopic tongue cancer model, anesthesia is associated with a risk of upper airway compromise due to posterior tongue displacement. Accordingly, *in vivo* bioluminescence imaging was performed at the minimum necessary frequency to reduce anesthesia-related risk. For IVIS imaging, anesthesia was induced and maintained with 2.0% isoflurane. Photon flux was quantified using fixed ROIs under standardized settings. Longitudinal analysis was restricted to days 1-15, when all mice were alive, and the signals remained within the linear range, to minimize signal saturation and attrition bias. Tumor presence was not assessed by any method other than IVIS during the experimental period because reliable palpation of mouse tongue tumors was not feasible. Tumor presence was confirmed only at the final necropsy, as confirmation of tumor mass formation required dissection. Mice were monitored daily for general health status and euthanized if body weight loss exceeded 20% or if severe debilitation occurred. Euthanasia was performed by cervical dislocation under isoflurane anesthesia on day 29 or earlier, if the humane endpoints were met, immediately after the final IVIS imaging while the mice remained anesthetized, and death was confirmed by the sustained absence of respiration and heartbeat. The cervical lymph nodes and lungs were harvested at necropsy, immersed in luciferin, and subjected to *ex vivo* BLI to detect metastases.

Tissues showing detectable *ex vivo* BLI signals were fixed in 10% neutral-buffered formalin, embedded in paraffin, and

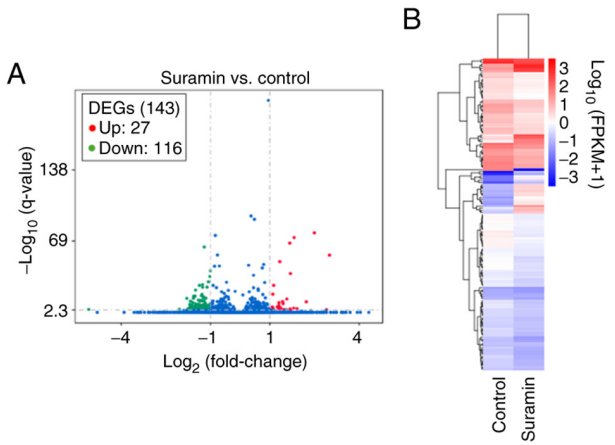

Figure 1. Differential gene expression in suramin-treated HSC-3 cells. (A) Volcano plot showing 143 differentially expressed genes (27 upregulated and 116 downregulated) between suramin-treated and control groups (llog$_2$ fold changel >1, q<0.005). (B) Heatmap showing hierarchical clustering of DEGs based on log$_{10}$ (FPKM + 1) values, which clearly distinguished suramin-treated from control cells. DEGs, differentially expressed genes; FPKM, fragments per kilobase of transcript per million mapped reads.

histologically examined to confirm the presence of metastatic SCC. Lymph nodes and lungs without detectable *ex vivo* BLI signals were not systematically examined. Because necropsies were performed at different time points owing to attrition, *ex vivo* metastasis measurements could not be temporally matched across animals. Metastasis was defined as a radiance value ≥3.0-fold above the background in the same animal, together with a discrete focal bioluminescence signal exhibiting a smooth intensity gradient.

Statistical analysis. Data are presented as mean ± SD with individual values. Enrichment analyses were considered significant at adjusted q<0.05 (Benjamini-Hochberg correction). A two-way mixed-effects model (REML with Geisser-Greenhouse correction) was used to evaluate the group, time, and interaction effects. Effect sizes were quantified as partial eta squared (partial η^2), and statistical significance was defined as P<0.05. All analyses were performed using GraphPad Prism 10.

Results

Suramin-induced transcriptomic alterations revealed by RNA-sequencing. RNA-sequencing detected 60,448 genes, of which 12,114 were commonly expressed in both groups. Differential expression analysis identified 116 downregulated and 27 upregulated genes in suramin-treated cells (Fig. 1A), and cluster analysis showed distinct expression patterns (Fig. 1B). Downregulated genes were dominated by regulators of the G_2/M transition and mitotic progression (e.g., *CCNB1*, *CDC20*, *AURKA*), kinetochore and spindle assembly (e.g., *CENPF*, *TPX*, *TUBB*), DNA metabolism (*RRM2* and *TK1*), chromatin regulation (*DNMT1*), cytokinesis (*ANLN*), chromosome segregation (*MKI67* and *TOP2A*), nuclear envelope integrity (*LMNB1/2*), DNA damage response (*HMGB1/2* and *PCNA*), and metabolic regulators (*LDHA* and *PSAT1*) were broadly suppressed (Table I).

In contrast, the upregulated genes encoded several matrix metalloproteinases (MMPs) with their inhibitor *TIMP3*, stress-response genes (*TXNIP* and *TP53INP1*), pro-apoptotic ligand *TNFSF10* (TRAIL), and immune-related regulators such as *PIK3IP1* and *FYB* (Table II).

GO enrichment analysis. GO enrichment analysis of the downregulated gene set demonstrated significant overrepresentation of mitosis-related pathways, including the mitotic cell cycle, DNA metabolic process, chromatin remodeling, and deoxyribonucleotide biosynthetic process, indicating the coordinated downregulation of genes governing G_2/M progression, DNA replication/repair, and chromatin regulation (Fig. 2A). In contrast, the upregulated genes were enriched in extracellular matrix-related processes, such as collagen catabolism, consistent with the activation of ECM remodeling (Fig. 2B).

KEGG analysis of differentially expressed genes. The KEGG pathway analysis demonstrated significant enrichment of pathways central to cell proliferation and genome stability in the downregulated gene set. The cell cycle was most prominently enriched, with associated terms involving G_2/M transition, spindle assembly, and checkpoint regulation. Additional enrichment in DNA replication, p53 signaling, and base excision repair supports the notion of impaired genome maintenance. Enrichment of cellular senescence, ubiquitin-mediated proteolysis, and apoptosis further indicated perturbation of protein turnover and checkpoint surveillance (Fig. 3A). In contrast, the upregulated genes were enriched in only three pathways, mineral absorption, IL-17 signaling, and lipid and atherosclerosis, suggesting adaptive changes in metal ion homeostasis, immune modulation, and lipid metabolism (Fig. 3B).

Protein-protein interaction network analysis. The PPI network of downregulated genes formed a densely interconnected module dominated by cell cycle and mitotic regulators. Hub genes included *CDK1*, *CCNA2*, *CCNB1*, *TOP2A*, *CDC20*, *KIF11*, *KIF20A*, *BUB1*, *PLK1*, *AURKB*, *TPX2*, and *CENPF*, all of which are central to the G_2/M transition, spindle function, and chromosome segregation (Table III).

In contrast, the network of upregulated genes was sparse, but revealed coherent submodules. Notably, MMPs, together with their inhibitor *TIMP3*, highlighted extracellular matrix remodeling, whereas *MT1E* and *MT2A* played roles in metal ion homeostasis and oxidative stress responses (Table III).

Transcription factor analysis. TFs were identified among the differentially expressed genes *FOXM1*, *MYBL2*, and *TCF19*. All three were significantly downregulated (*FOXM1*, FDR=5.01x10^{-6}, log$_2$FC=-1.27; *MYBL2*, FDR=1.58x10^{-5}, log$_2$FC=-1.65; *TCF19*, FDR=1.71x10^{-5}, log$_2$FC=-1.53). Binding motifs for *FOXM1* and *MYBL2* were validated in JASPAR 2024, and their binding activity was further supported by ENCODE ChIP-seq datasets. In contrast, *TCF19* lacked motif evidence and demonstrated only limited ChIP-seq support. Therefore, it was regarded as putative in this context.

Effects of suramin treatment in an orthotopic tongue cancer mouse model. Although five mice per group were initially

Table I. Top 30 downregulated genes identified by mRNA-sequencing in suramin-treated HSC-3 cells.

Rank	Gene symbol	Known function	Fold change	q-value
1	*TUBB*	Microtubule component	0.43	4.61×10^{-64}
2	*LDHA*	Glycolysis, lactate production, Warburg effect	0.50	5.32×10^{-41}
3	*EIF5A*	Translation elongation, mRNA turnover	0.49	1.85×10^{-35}
4	*HMGB1*	Chromatin remodeling, DAMPs	0.48	2.30×10^{-30}
5	*TUBB4B*	Microtubule assembly	0.42	1.42×10^{-27}
6	*LMNB2*	Nuclear lamina component	0.39	7.51×10^{-27}
7	*TOP2A*	DNA topology, mitotic chromosome condensation	0.46	3.31×10^{-25}
8	*MKI67*	Chromatin organization, cell proliferation	0.42	4.51×10^{-25}
9	*UBE2S*	Ubiquitination, mitotic progression	0.35	2.29×10^{-22}
10	*TUBA1C*	Microtubule assembly	0.41	3.88×10^{-18}
11	*KPNA2*	Nuclear import	0.40	6.47×10^{-17}
12	*CCNB1*	G2/M transition	0.35	1.43×10^{-16}
13	*CDC20*	Anaphase-promoting complex activator	0.34	2.30×10^{-16}
14	*HMGB2*	Chromatin remodeling,	0.42	6.15×10^{-16}
15	*RRM2*	dNTP synthesis, DNA replication	0.34	1.59×10^{-15}
16	*RANBP1*	Nucleocytoplasmic transport	0.42	5.75×10^{-15}
17	*DNMT1*	DNA methylation maintenance	0.45	1.43×10^{-14}
18	*TK1*	dTTP synthesis, DNA replication	0.34	1.96×10^{-14}
19	*TUBA1B*	Microtubule assembly	0.29	2.16×10^{-14}
20	*ANLN*	Cytokinesis, actin cytoskeleton regulation	0.38	1.03×10^{-12}
21	*TCOF1*	rRNA processing	0.40	1.32×10^{-12}
22	*LMNB1*	Nuclear lamina structure	0.40	6.85×10^{-12}
23	*CENPF*	Kinetochore function, chromosome segregation	0.43	6.95×10^{-12}
24	*TPX2*	Spindle assembly, microtubule nucleation	0.42	8.74×10^{-12}
25	*PSAT1*	Serine biosynthesis	0.31	1.19×10^{-11}
26	*CKS1B*	CDK regulation, cell cycle	0.39	1.96×10^{-11}
27	*AURKA*	Mitotic spindle, centrosome maturation	0.33	3.28×10^{-10}
28	*PCNA*	DNA replication and repair	0.45	1.65×10^{-9}
29	*HNRNPAB*	Pre-mRNA processing, mRNA transport	0.49	6.15×10^{-9}
30	*CKS2*	CDK regulation, cell cycle progression	0.35	6.31×10^{-9}

CDK, cyclin-dependent kinase; DAMPs, damage-associated molecular patterns; dNTP, deoxyribonucleoside triphosphate; dTTP, deoxythymidine triphosphate.

enrolled, early accidental deaths resulted in four mice in the vehicle group and five in the 20 mg/kg group available for longitudinal analyses. Body weights were measured during IVIS imaging and suramin administration. Mice were regularly monitored, and euthanasia was performed at humane endpoints (>20% body weight loss with progressive debilitation due to tumor burden). Accordingly, analyses were restricted to day 15, when all the mice remained alive, and the BLI signals were within the linear detection range. Although BLI values were lower in the suramin 20 mg/kg group than in the vehicle group at this time point, the mixed-effects model did not detect a significant group effect (P=0.22), or a significant time x group interaction (P=0.18). Effect size estimates were relatively large for both the group effect (partial η^2=0.20) and the time x group interaction (partial η^2=0.24), but were insufficient to establish a clear inhibitory effect of suramin (Fig. 4A and B). In contrast, tumor growth in the suramin 60 mg/kg group was comparable to that in the vehicle group, and no difference was detected (Fig. S1A and B). Further studies with larger cohorts are necessary to determine whether suramin exerts a measurable influence on tumor progression. Data collected after day 15 were excluded from the quantitative analysis owing to signal saturation and attrition. Lymph node metastases were detected in the 60 mg/kg (day 22), 20 mg/kg (day 25), and vehicle groups (two cases on day 29). Pulmonary metastasis was detected in one vehicle-treated group on day 29. Because necropsies were performed at different time points, the timing and frequency of metastases could not be statistically evaluated. The final confirmation of metastasis was based on *ex vivo* BLI during necropsy. The mixed-effects model up to day 22 demonstrated a significant main effect of time (P=0.0006), whereas neither the group effect (P=0.16) nor the time x group interaction (P=0.36) was significant. Although statistical group differences were not demonstrated, the 60 mg/kg group began to show a marked decline

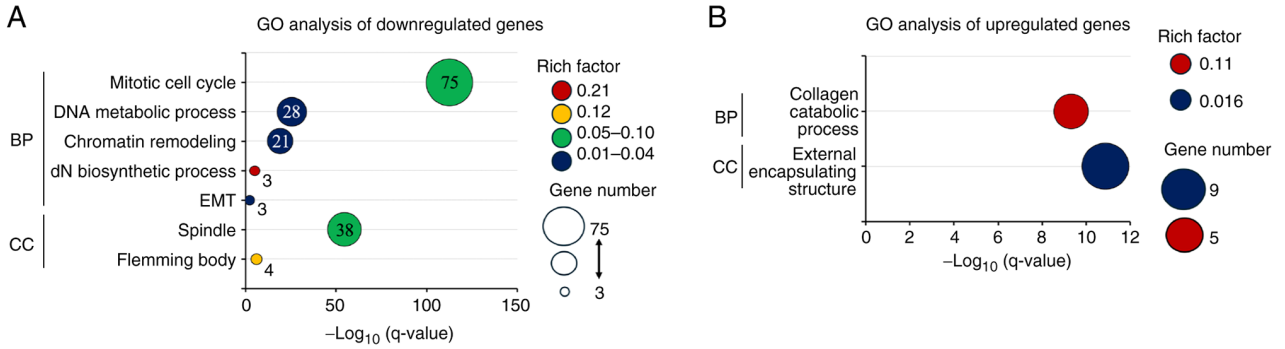

Figure 2. GO enrichment analysis of differentially expressed genes. (A) Downregulated genes were significantly enriched in GO terms related to the cell cycle and mitotic progression within the BP and CC categories. (B) Upregulated genes were enriched in GO terms associated with extracellular matrix organization and stress response. In both panels, the x-axis represents the rich factor, bubble size indicates the number of genes, and bubble color reflects -$\log_{10}$ (q-value). BP, biological process; CC, cellular component; GO, Gene Ontology.

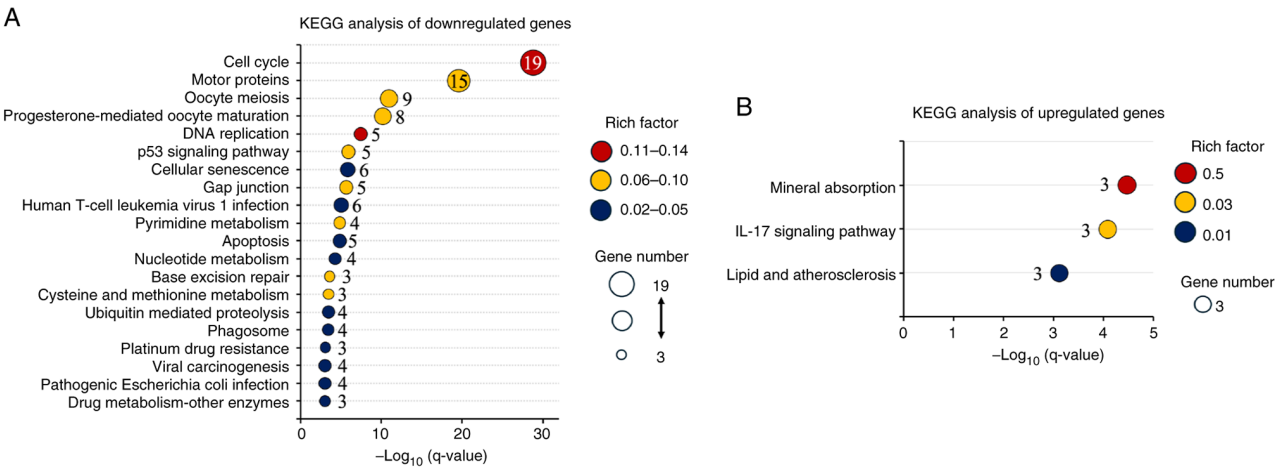

Figure 3. KEGG pathway enrichment analysis of differentially expressed genes. (A) Downregulated genes were significantly enriched in pathways related to the cell cycle, DNA replication, and other proliferation-associated processes. (B) Upregulated genes were enriched in pathways associated with extracellular matrix remodeling and stress response. In both panels, the x-axis represents the rich factor, bubble size indicates the number of genes, and bubble color reflects -$\log_{10}$ (q-value). KEGG, Kyoto Encyclopedia of Genes and Genomes.

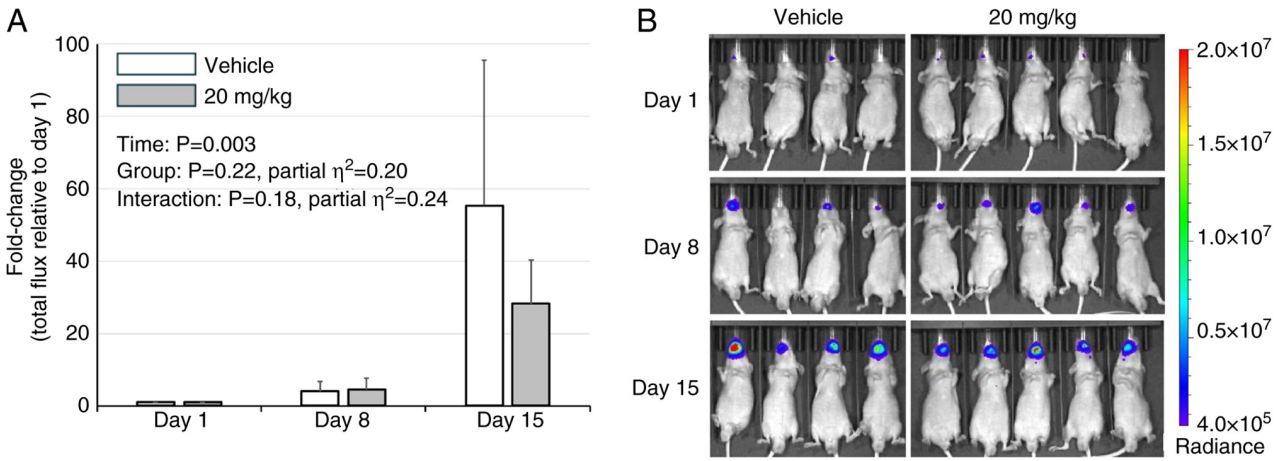

Figure 4. *In vivo* effects of suramin on tumor growth in an orthotopic tongue squamous cell carcinoma model. (A) BLI signals relative to day 1 are shown for vehicle- and 20 mg/kg-treated groups. Suramin administration at 20 mg/kg was associated with reduced tumor growth compared with vehicle, although the difference was not statistically significant. (B) *In vivo* bioluminescence images of orthotopic HSC-3-Luc tumors in the vehicle and Suramin (20 mg/kg) groups.

from day 18, and one mouse died by day 21, supporting clear systemic toxicity at a high dose (Fig. S2). *Ex vivo* BLI confirmed the metastatic involvement of the cervical lymph nodes and lungs. The corresponding radiance values and

Table II. The 27 upregulated genes identified by mRNA-sequencing in suramin-treated HSC-3 cells.

Rank	Gene symbol	Known function	Fold change	q-value
1	*MMP10*	ECM degradation	5.63	1.16×10^{-77}
2	*MMP1*	ECM degradation, invasion	3.52	3.18×10^{-73}
3	*CLU*	Apoptosis modulation, extracellular chaperone	3.17	9.02×10^{-68}
4	*MMP13*	ECM degradation, collagen degradation	8.02	3.43×10^{-56}
5	*TXNIP*	Oxidative stress response, redo regulation	2.52	6.30×10^{-50}
6	*CLDN1*	Tight junctions, epithelial barrier	3.22	2.25×10^{-38}
7	*GLUL*	Metabolic adaptation, glutamine synthesis	2.18	7.04×10^{-27}
8	*MT2A*	Metal ion homeostasis, oxidative stress response	2.14	2.62×10^{-18}
9	*CYBRD1*	Iron metabolism, ferric reductase activity	2.96	9.73×10^{-14}
10	*CCDC80*	Cell adhesion, matrix assembly	2.68	3.69×10^{-11}
11	*MMP12*	ECM degradation, elastin remodeling	4.67	5.89×10^{-11}
12	*TIMP3*	MMP inhibition, ECM stabilization	2.47	4.20×10^{-10}
13	*FBXO32*	E3 ligase, protein degradation	2.71	3.74×10^{-9}
14	*PTGES*	PGE_2 synthesis, inflammatory response	2.47	2.96×10^{-7}
15	*PIK3IP1*	Negative regulator of PI3K	2.37	3.38×10^{-6}
16	*PLEKHA6*	PH domain-containing protein	2.12	5.33×10^{-6}
17	*DHRS3*	Retinal to retinol reduction	2.57	4.47×10^{-5}
18	*FYB*	T-cell signaling adaptor	3.48	7.23×10^{-5}
19	*TNFSF10*	Apoptosis induction	2.15	8.09×10^{-5}
20	*TP53INP1*	Stress-induced apoptosis	3.76	1.87×10^{-4}
21	*KLHL24*	BCR E3 ligase complex	2.44	1.88×10^{-4}
22	*NATD1*	Acetyltransferase domain-containing protein	2.58	2.14×10^{-4}
23	*MMP3*	ECM degradation	3.19	3.75×10^{-4}
24	*MT1E*	Heavy metal binding	2.77	1.37×10^{-3}
25	*TG*	Substrate for thyroid hormone synthesis	3.22	1.66×10^{-3}
26	*CTSF*	Intracellular degradation, turnover of proteins	7.46	1.78×10^{-3}
27	*ITGB8*	RGD recognition	2.94	2.32×10^{-3}

BCR, BTB-CUL3-RBX1; ECM, extracellular matrix; MMP, matrix metalloproteinase; PGE_2, prostaglandin E_2; PH, pleckstrin homology; PI3K, phosphatidylinositol 3-kinase; RGD, arginine-glycine-aspartic acid.

images are provided in Table SI and Fig. S3. In the 20 mg/kg group, metastasis was not counted in mouse #5 because the lung signal lacked a smooth intensity gradient and was judged as background rather than a discrete metastatic focus based on the predetermined imaging criteria (Fig. S3).

Discussion

Transcriptomic reprogramming induced by suramin in TSCC cells highlights a dual antitumor mechanism: suppression of proliferative networks and modulation of the tumor microenvironment. On the proliferative side, broad downregulation of genes essential for the G_2/M transition (e.g., *CCNB1*, *CDC20*, *AURKA*) and spindle assembly (e.g., *TPX2*, *TUBA1C*, *TUBB4B*) indicates impaired mitotic entry, chromosome segregation, and spindle formation. This aligns with previous findings that suramin induces G_2/M arrest in breast cancer cells (12), suggesting a conserved mechanism of cell cycle inhibition across different malignancies.

Our previous study demonstrated that suramin reduces the HuR-mediated stabilization of *CCNB1* and *CCNA2* (7). Although *CCNA2* was not listed among the top 30 downregulated genes, it ranked 55th among 116 downregulated genes. In addition, other HuR-stabilized transcripts, such as *HMGB1, RRM2,* and *DNMT1*, reported in previous studies, were also downregulated in the present dataset (13-15). This concordance between known HuR-dependent transcripts and the current RNA-seq results supports HuR inhibition as a contributing mechanism.

In parallel, suramin reprogrammed transcriptional pathways related to extracellular matrix remodeling. Upregulation of several MMPs, together with *TIMP3*, may indicate a more regulated ECM-associated transcriptional program, distinct from the unchecked MMP/TIMP imbalance typical of aggressive tumors (16-18). The co-upregulation of *MMP9*, *MMP11*, and *MMP14* with *TIMP3* has been regarded as a failed compensatory response in advanced ovarian cancer (19), whereas in cartilage models, suramin suppresses *MMP13* while inducing *TIMP3,* exerting protective ECM effects (20,21). Taken together, these observations indicate that suramin is consistent with a balanced ECM remodeling-related transcriptional program in TSCC. However, the functional consequences of this MMP/*TIMP3*

Table III. Top 30 downregulated and upregulated genes based on degree centrality in the PPI network.

A, Downregulated genes

Rank	Gene symbol	Degree
1	*CDK1*	77
2	*CCNA2*	71
3	*CCNB1*	70
4	*TOP2A*	69
5	*CDC20*	67
6	*KIF11*	67
7	*KIF20A*	66
8	*BUB1*	66
9	*PLK1*	65
10	*DLGAP5*	64
11	*AURKB*	63
12	*BUB1B*	62
13	*TPX2*	62
14	*CCNB2*	61
15	*BIRC5*	61
16	*KIF2C*	61
17	*AURKA*	60
18	*KIF4A*	60
19	*CDCA8*	60
20	*CENPF*	59
21	*UBE2C*	59
22	*ASPM*	59
23	*KIF23*	57
24	*NUSAP1*	57
25	*CEP55*	56
26	*MELK*	56
27	*CENPA*	55
28	*PBK*	55
29	*NCAPG*	54
30	*RRM2*	54

B, Upregulated genes

Rank	Gene symbol	Degree
1	*MMP3*	4
2	*MMP1*	3
3	*TIMP3*	3
4	*MMP10*	2
5	*MMP12*	1
6	*MMP13*	1
7	*MT1E*	1
8	*MT2A*	1

pattern were not evaluated in this exploratory study, and this interpretation should, therefore, be regarded as tentative.

Suramin also enhances the stress- and immune-adaptive pathways. Upregulation of *TXNIP*, *MT1E*, and *MT2A* indicates reinforcement of oxidative stress responses; *TXNIP* promotes oxidative stress and apoptosis (22), *MT2A* protects against oxidative injury (23), and *MT1E*, which is often silenced in cancers such as HCC (24,25), was re-induced, consistent with tumor-suppressive reprogramming. Pro-apoptotic mediators (*TNFSF10* and *TP53INP1*) (26,27), the PI3K pathway inhibitor *PIK3IP1* (28,29), and the immune adaptor *FYB* (30) were also upregulated, suggesting broad modulation of apoptosis and immune-related processes.

Our PPI network analysis supported this dual reprogramming: a densely connected mitotic module was suppressed, whereas smaller yet coherent subnetworks related to ECM remodeling and stress responses were activated, consistent with the modular reorganization reported in cancer systems biology (31).

Importantly, transcription factor analysis revealed the concurrent downregulation of *MYBL2*, which cooperates with the DREAM complex to initiate late S/G2 transcription, and *FOXM1*, the master regulator of G_2/M progression (32). *TCF19*, another repressed factor, promotes β-cell stress survival partly through *FOXM1* regulation (33) and promotes proliferation and tumor formation in lung carcinoma by activating the RAF/MEK/ERK pathway (34). Thus, the suramin-mediated suppression of *TCF19* may synergize with *MYBL2*/*FOXM1* repression, reinforcing the collapse of mitotic transcriptional programs and contributing to anti-invasive reprogramming. Taken together, these findings support a dual mechanism of action: profound suppression of mitotic progression and regulation of the tumor microenvironment (35).

Multiple studies have reported diverse suramin dosing regimens and antitumor effects, reflecting its dual role as a direct cytotoxic agent at high doses and as a chemosensitizer at low exposures. In preclinical models, high-dose monotherapy (~60 mg/kg per injection) suppressed tumor growth, including in human osteosarcoma xenografts (36). In contrast, lower-dose schedules (5-10 mg/kg, twice weekly) are commonly employed to enhance the efficacy of paclitaxel, docetaxel, doxorubicin, and cisplatin with minimal added toxicity (37,38).

In our orthotopic TSCC model, suramin administered at 20 mg/kg twice weekly reduced tumor growth, although statistical significance (P=0.18) was not achieved because of the limited cohort size; the effect size was relatively large (partial η^2=0.24). This dosing range was selected based on previous reports indicating that the intraperitoneal administration of up to 60 mg/kg in mice yielded pharmacologically active systemic exposure, although plasma suramin levels were not measured in this study. This finding is broadly consistent with previous reports of *in vivo* activity, including significant growth inhibition of DU145 prostate cancer xenografts with suramin monotherapy at effective doses (39) and enhanced inhibition of ovarian cancer xenografts when combined with cisplatin (38). Furthermore, previous *in vitro* studies, including our own report (7), have demonstrated that suramin suppresses the proliferation and invasion of oral squamous cell carcinoma cells, including our own report (7), supporting the notion that suramin exerts multifaceted antitumor effects in oral cancer. When contextualized using body surface-area scaling (40), the 20 and 60 mg/kg doses in mice fell within the clinically explored dosing range; however, such a conversion provides only a theoretical estimate and does not

predict plasma exposure or toxicity. However, in our model, the 60 mg/kg regimen was associated with more pronounced adverse effects than the 20 mg/kg regimen. This was accompanied by marked body weight loss, indicating high toxicity at this dose. At excessively high doses, further increases in antitumor efficacy may not necessarily occur, and several angiogenesis- and immune-related anticancer agents have been reported to exhibit non-linear dose-response relationships in which the therapeutic benefit plateaus or declines beyond an optimal window (41). Although this phenomenon has not been established for suramin, the substantial toxicity observed at 60 mg/kg in our model raises the possibility that excessively high exposure may limit the therapeutic benefits. The assessment of metastasis was limited because the mouse numbers declined as early as day 21 in the 60 mg/kg group and from day 23 in the 20 mg/kg and vehicle groups. Because lymph node metastases typically appeared after day 25, a reliable evaluation would require a larger number of mice to ensure sufficient survival in the later phase of tumor progression. *Ex vivo* BLI findings of lymph nodes and lungs are presented in the supplementary data for completeness; however, differences in necropsy timing prevent quantitative comparison of the metastatic burden.

Suramin dosing is clinically guided by a nomogram. Regimens targeting non-cytotoxic plasma concentrations (10-50 μM for ≥48 h) were primarily applied in combination chemotherapy trials, where suramin enhanced the effects of agents such as paclitaxel and carboplatin (42). In contrast, a large randomized Phase III trial in HRPC employed dosing schedules designed to maintain plasma concentrations within the range of 100-300 μg/ml together with hydrocortisone (8). This approach produced a modest symptomatic benefit but no survival advantage, and the overall incidence of severe adverse events, including neurotoxicity, was relatively low owing to careful pharmacokinetic control (8). Earlier studies, however, demonstrated that when plasma concentrations exceeded 350 μg/ml, the risk of dose-limiting neurotoxicity increased substantially (43). A more recent clinical pharmacokinetic study reported that a single 20 mg/kg infusion in humans produced peak plasma concentrations close to this level (C_{max}=328 μg/ml), without exceeding the upper boundary of the recommended therapeutic window (44). Collectively, these results suggest that suramin is unlikely to be effective as a single agent but may have substantial value as a chemosensitizer in rational combination regimens. This finding warrants further validation in larger preclinical cohorts.

Suramin also exhibits anti-inflammatory activity in addition to its antitumor effects. In a DNCB-induced atopic dermatitis mouse model, intraperitoneal administration at 20 mg/kg twice weekly for 3 weeks significantly reduced serum IL-6, IL-1β, TNF-α, and IgE, improving dermatitis scores (45). These effects are plausibly linked to the blockade of HMGB1/HMGB2 signaling, as suramin's broad polyanionic interactions can neutralize cationic DAMPs, such as HMGB1 and extracellular histones, providing a mechanistic rationale for its dual anti-inflammatory and antitumor activities.

In conclusion, this study demonstrates that suramin exerts a dual antitumor effect in TSCC by suppressing proliferative regulators such as *MYBL2*, *FOXM1*, and *TCF19*, thereby impairing the G_2/M transition, while activating pathways associated with ECM remodeling and stress responses. In our orthotopic TSCC model, 20 mg/kg suramin reduced tumor growth compared to controls without achieving statistical significance; however, the relatively large effect size highlights suramin as a promising candidate for further translational investigation.

This study is exploratory, relying on single-sample transcriptomics and a small *in vivo* cohort. The *in vivo* analysis was limited to day 15 due to signal saturation and attrition, which precluded the evaluation of longer-term effects. Functional validation of key findings-including G_2/M arrest, *FOXM1*/*MYBL2* activity, and the MMP/*TIMP3* profile-was not performed. Accordingly, the present findings should be interpreted as hypothesis-generating and require validation in larger, adequately powered studies. In addition, systematic toxicity scoring was not performed, limiting quantitative evaluation of dose-related tolerability, and hub genes identified by the PPI network were not validated at the protein level by western blotting. Future studies using ChIP-qPCR to directly assess FOXM1/MYBL2 binding to target gene promoters, as well as validation in additional TSCC and HNSCC cell lines, will be required to determine whether the observed transcriptomic changes are not cell-line-specific.

Acknowledgements

The authors would like to thank Dr Takashi Murakami (Department of Microbiology, Saitama Medical University, Moroyama, Japan) for kindly providing the luciferase-expressing HSC-3 cells used in this study. This work was also supported by the infrastructure and equipment at GI-CoRE GSQ, Hokkaido University (Sapporo, Japan).

Funding

This work was supported by the Japan Society for the Promotion of Science KAKENHI (grant nos. JP18K17022, JP22K09922, and JP25K12969).

Availability of data and materials

The RNA-sequencing data generated in the present study may be found in the NCBI BioProject database under accession number PRJNA1347865 or at the following URL: https://www.ncbi.nlm.nih.gov/bioproject/?term=PRJNA1347865. All other data generated in the present study may be requested from the corresponding author.

Authors' contributions

WK designed the study, performed RNA extraction, animal experiments and bioinformatics analyses, interpreted the data and drafted the manuscript. MM performed and analyzed the animal experiments. NM and KH contributed to the design and analysis of the animal experiments. KT contributed to the acquisition of animal experimental data, including data collection. TN, SO and KM contributed to the interpretation and discussion of the suramin-related data. YO contributed to the analysis and interpretation of data. WK and YO confirms the authenticity of all the raw data. All authors have read and approved the final manuscript.

Ethics approval and consent to participate

All procedures were approved by the Institutional Animal Care and Use Committee of Hokkaido University (approval no. 18-0050; Sapporo, Japan) and conducted in accordance with the institutional guidelines for animal welfare.

Patient consent for publication

Not applicable.

Competing interests

The authors declare that they have no competing interests.

Use of artificial intelligence tools

During the preparation of this work, AI tools (ChatGPT) were used to improve the readability and language of the manuscript, and subsequently, the authors revised and edited the content produced by the AI tools as necessary, taking full responsibility for the ultimate content of the present manuscript.

References

1. Coropciuc R, Moreno-Rabié C, De Vos W, Van de Casteele E, Marks L, Lenaerts V, Coppejans E, Lenssen O, Coopman R, Walschap J, *et al*: Navigating the complexities and controversies of medication-related osteonecrosis of the jaw (MRONJ): A critical update and consensus statement. Acta Chir Belg 124: 1-11, 2024.
2. National Comprehensive Cancer Network (NCCN): NCCN Clinical Practice Guidelines in Oncology: Head and Neck Cancers. Version 1.2026. NCCN, Plymouth Meeting, PA, 2026. https://www.nccn.org. Accessed January 8, 2026.
3. Steverding D and Troeberg L: 100 years since the publication of the suramin formula. Parasitol Res 123: 11, 2023.
4. Wiedemar N, Hauser DA and Mäser P: 100 years of suramin. Antimicrob Agents Chemother 64: e01168-19, 2020.
5. Zaragoza-Huesca D, Rodenas MC, Peñas-Martínez J, Pardo-Sánchez I, Peña-García J, Espín S, Ricote G, Nieto A, García-Molina F, Vicente V, *et al*: Suramin, a drug for the treatment of trypanosomiasis, reduces the prothrombotic and metastatic phenotypes of colorectal cancer cells by inhibiting hepsin. Biomed Pharmacother 168: 115814, 2023.
6. Naviaux RK, Curtis B, Li K, Naviaux JC, Bright AT, Reiner GE, Westerfield M, Goh S, Alaynick WA, Wang L, *et al*: Low-dose suramin in autism spectrum disorder: A small, phase I/II, randomized clinical trial. Ann Clin Transl Neurol 4: 491-505, 2017.
7. Kakuguchi W, Nomura T, Kitamura T, Otsuguro S, Matsushita K, Sakaitani M, Maenaka K and Tei K: Suramin, screened from an approved drug library, inhibits HuR functions and attenuates malignant phenotype of oral cancer cells. Cancer Med 7: 6269-6280, 2018.
8. Small EJ, Meyer M, Marshall ME, Reyno LM, Meyers FJ, Natale RB, Lenehan PF, Chen L, Slichenmyer WJ and Eisenberger M: Suramin therapy for patients with symptomatic hormone-refractory prostate cancer: Results of a randomized phase III trial comparing suramin plus hydrocortisone to placebo plus hydrocortisone. J Clin Oncol 18: 1440-1450, 2000.
9. Cheng B, Gao F, Maissy E and Xu P: Repurposing suramin for the treatment of breast cancer lung metastasis with glycol chitosan-based nanoparticles. Acta Biomater 84: 378-390, 2019.
10. Wang L, Feng Z, Wang X and Zhang X: DEGseq: An R package for identifying differentially expressed genes from RNA-seq data. Bioinformatics 26: 136-138, 2010.
11. Young TR, Yamamoto M, Kikuchi SS, Yoshida AC, Abe T, Inoue K, Johansen JP, Benucci A, Yoshimura Y and Shimogori T: Thalamocortical control of cell-type specificity drives circuits for processing whisker-related information in mouse barrel cortex. Nat Commun 14: 6077, 2023.
12. Foekens JA, Sieuwerts AM, Stuurman-Smeets EM, Peters HA and Klijn JG: Effects of suramin on cell-cycle kinetics of MCF-7 human breast cancer cells in vitro. Br J Cancer 67: 232-236, 1993.
13. Al-Kharashi LA, Al-Mohanna FH, Tulbah A and Aboussekhra A: The DNA methyl-transferase protein DNMT1 enhances tumor-promoting properties of breast stromal fibroblasts. Oncotarget 9: 2329-2343, 2017.
14. Zhang J, Wu Q, Xie Y, Li F, Wei H, Jiang Y, Qiao Y, Li Y, Sun Y, Huang H, *et al*: Ribonucleotide reductase small subunit M2 promotes the proliferation of esophageal squamous cell carcinoma cells carcinoma cells via HuR-mediated mRNA stabilization. Acta Pharm Sin B 14: 4329-4344, 2024.
15. Wang J, Zhao L, Li Y, Feng S and Lv G: HuR induces inflammatory responses in HUVECs and murine sepsis via binding to HMGB1. Mol Med Rep 17: 1049-1056, 2018.
16. Stetler-Stevenson WG: The tumor microenvironment: regulation by MMP-independent effects of tissue inhibitor of metalloproteinases-2. Cancer Metastasis Rev 27: 57-66, 2008.
17. Brew K and Nagase H: The tissue inhibitors of metalloproteinases (TIMPs): An ancient family with structural and functional diversity. Biochim Biophys Acta 1803: 55-71, 2010.
18. Cabral-Pacheco GA, Garza-Veloz I, Castruita-De la Rosa C, Ramirez-Acuña JM, Perez-Romero BA, Guerrero-Rodriguez JF, Martinez-Avila N and Martinez-Fierro ML: The roles of matrix metalloproteinases and their inhibitors in human diseases. Int J Mol Sci 21: 9739, 2020.
19. Escalona RM, Kannourakis G, Findlay JK and Ahmed N: Expression of TIMPs and MMPs in ovarian tumors, ascites, ascites-derived cells, and cancer cell lines: Characteristic modulatory response before and after chemotherapy treatment. Front Oncol 11: 796588, 2022.
20. Guns LA, Monteagudo S, Kvasnytsia M, Kerckhofs G, Vandooren J, Opdenakker G, Lories RJ and Cailotto F: Suramin increases cartilage proteoglycan accumulation in vitro and protects against joint damage triggered by papain injection in mouse knees in vivo. RMD Open 3: e000604, 2017.
21. Chanalaris A, Doherty C, Marsden BD, Bambridge G, Wren SP, Nagase H and Troeberg L: Suramin inhibits osteoarthritic cartilage degradation by increasing extracellular levels of chondroprotective tissue inhibitor of metalloproteinases 3. Mol Pharmacol 92: 459-468, 2017.
22. Deng J, Pan T, Liu Z, McCarthy C, Vicencio JM, Cao L, Alfano G, Suwaidan AA, Yin M, Beatson R and Ng T: The role of TXNIP in cancer: A fine balance between redox, metabolic, and immunological tumor control. Br J Cancer 129: 1877-1892, 2023.
23. Ling XB, Wei HW, Wang J, Kong YQ, Wu YY, Guo JL, Li TF and Li JK: Mammalian metallothionein-2a and oxidative stress. Int J Mol Sci 17: 1483, 2016.
24. Si M and Lang J: The roles of metallothioneins in carcinogenesis. J Hematol Oncol 11: 107, 2018.
25. Liu Q, Lu F and Chen Z: Identification of MT1E as a novel tumor suppressor in hepatocellular carcinoma. Pathol Res Pract 216: 153213, 2020.
26. Niroshika KKH, Weerakoon K, Molagoda IMN, Samarakoon KW, Weerakoon HT and Jayasooriya RGPT: Exploring the dynamic role of circulating soluble tumor necrosis factor-related apoptosis-inducing ligand (TRAIL) as a diagnostic and prognostic marker; a review. Biochem Biophys Res Commun 751: 151415, 2025.
27. Deng Y, Li AM, Zhao XM, Song ZJ and Liu SD: Downregulation of tumor protein 53-inducible nuclear protein 1 expression in hepatocellular carcinoma correlates with poor prognosis. Oncol Lett 13: 1228-1234, 2017.
28. He X, Zhu Z, Johnson C, Stoops J, Eaker AE, Bowen W and DeFrances MC: PIK3IP1, a negative regulator of PI3K, suppresses the development of hepatocellular carcinoma. Cancer Res 68: 5591-5598, 2008.
29. Uche UU, Piccirillo AR, Kataoka S, Grebinoski SJ, D'Cruz LM and Kane LP: PIK3IP1/TrIP restricts activation of T cells through inhibition of PI3K/Akt. J Exp Med 215: 3165-3179, 2018.
30. Peterson EJ, Woods ML, Dmowski SA, Derimanov G, Jordan MS, Wu JN, Myung PS, Liu QH, Pribila JT, Freedman BD, *et al*: Coupling of the TCR to integrin activation by Slap-130/Fyb. Science 293: 2263-2265, 2001.
31. Chuang HY, Lee E, Liu YT, Lee D and Ideker T: Network-based classification of breast cancer metastasis. Mol Syst Biol 3: 140, 2007.
32. Sadasivam S and DeCaprio JA: The DREAM complex: Master coordinator of cell cycle-dependent gene expression. Nat Rev Cancer 13: 585-595, 2013.

33. Krautkramer KA, Linnemann AK, Fontaine DA, Whillock AL, Harris TW, Schleis GJ, Truchan NA, Marty-Santos L, Lavine JA, Cleaver O, *et al*: Tcf19 is a novel islet factor necessary for proliferation and survival in the INS-1 β-cell line. Am J Physiol Endocrinol Metab 305: E600-E610, 2013.
34. Tian Y, Xin S, Wan Z, Dong H, Liu L, Fan Z, Li T, Peng F, Xiong Y and Han Y: TCF19 promotes cell proliferation and tumor formation in lung cancer by activating the Raf/MEK/ERK signaling pathway. Transl Oncol 45: 101978, 2024.
35. Egeblad M and Werb Z: New functions for the matrix metalloproteinases in cancer progression. Nat Rev Cancer 2: 161-174, 2002.
36. Walz TM, Abdiu A, Wingren S, Smeds S, Larsson SE and Wasteson A: Suramin inhibits growth of human osteosarcoma xenografts in nude mice. Cancer Res 51: 3585-3589, 1991.
37. Zhang Y, Song S, Yang F, Au JL and Wientjes MG: Nontoxic doses of suramin enhance activity of doxorubicin in prostate tumors. J Pharmacol Exp Ther 299: 426-433, 2001.
38. Kikuchi Y, Hirata J, Hisano A, Tode T, Kita T and Nagata I: Complete inhibition of human ovarian cancer xenografts in nude mice by suramin and cis-diamminedichloroplatinum(II). Gynecol Oncol 58: 11-15, 1995.
39. Church D, Zhang Y, Rago R and Wilding G: Efficacy of suramin against human prostate carcinoma DU145 xenografts in nude mice. Cancer Chemother Pharmacol 43: 198-204, 1999.
40. Nair AB and Jacob S: A simple practice guide for dose conversion between animals and human. J Basic Clin Pharm 7: 27-31, 2016.
41. Reynolds AR: Potential relevance of bell-shaped and u-shaped dose-responses for the therapeutic targeting of angiogenesis in cancer. Dose Response 8: 253-284, 2010.
42. Chen D, Song SH, Wientjes MG, Yeh TK, Zhao L, Villalona-Calero M, Otterson GA, Jensen R, Grever M, Murgo AJ and Au JL: Nontoxic suramin as a chemosensitizer in patients: dosing nomogram development. Pharm Res 23: 1265-1274, 2006.
43. Chaudhry V, Eisenberger MA, Sinibaldi VJ, Sheikh K, Griffin JW and Cornblath DR: A prospective study of suramin-induced peripheral neuropathy. Brain 119 (Pt 6): 2039-2052, 1996.
44. Wu G, Zhou H, Lv D, Zheng R, Wu L, Yu S, Kai J, Xu N, Gu L, Hong N and Shentu J: Phase I, single-dose study to assess the pharmacokinetics and safety of suramin in healthy Chinese volunteers. Drug Des Devel Ther 17: 2051-2061, 2023.
45. Alyoussef A: Suramin attenuated inflammation and reversed skin tissue damage in experimentally induced atopic dermatitis in mice. Inflamm Allergy Drug Targets 13: 406-410, 2015.